Proceedings of the 21st ICSMGE, Vienna, Austria, 14 – 19 June 2026. Pistrol, Adam & Schweiger (eds.)
Published by: ÖGG, Austrian Society for Geomechanics, Salzburg, Austria, ISBN 978-3-9503898-4-5
https://doi.org/10.53243/ICSMGE2026-235

Numerical study on the bearing behaviour of piled rafts under seismic loading

Yimer Degu
Department of Geotechnical Engineering, University of Kassel, Kassel, Germany, and Faculty of Civil and Water Resources Engineering, Bahir Dar Institute of Technology, Bahir Dar University, Bahir Dar, Ethiopia, yideg@uni-kassel.de

Oliver Reul
Department of Geotechnical Engineering, University of Kassel, Kassel, Germany

Asrat Worku
School of Civil and Environmental Engineering, College of Technology and Built Environment, Addis Ababa University, Addis Ababa, Ethiopia

Franz Tschuchnigg
Institute of Soil Mechanics, Foundation Engineering and Computational Geotechnics, Graz University of Technology, Graz, Austria

ABSTRACT: Piled rafts are well-established foundation systems, especially for tall buildings under predominantly vertical static loading. For this load case, a guideline for dimensioning, design and construction of piled rafts termed as Combined Pile-Raft Foundations (CPRF) already exists. However, in contrast to piled rafts under vertical loading, limited knowledge is available on the soil-structure interaction of piled rafts under combined vertical and horizontal loading, regardless of whether monotonic, cyclic or dynamic actions are involved. This paper aims at providing an insight into the bearing behaviour of bridge piers founded on piled rafts under dynamic loading by means of 3D finite element analysis (3D FEA). To simulate the nonlinear behaviour of the soil, the Hardening Soil model with small-strain stiffness (HSsmall) is employed, which was calibrated by means of a back analysis of centrifuge tests. Parametric studies were performed to assess the impact of various factors on the settlement, lateral displacement, acceleration, response spectra, load share between piles and raft, and dynamic response of the piled raft. Within the scope of this paper, the influence of key factors, including kinematic and inertial interactions, pile configuration and geometry (spacing, diameter, and length) and loading conditions, on the bearing behaviour of piled rafts under seismic loading is discussed.

KEYWORDS: bridge pier, piled raft, seismic loading, 3D finite element analysis, HSsmall soil model.

1 INTRODUCTION

For tall buildings under predominantly vertical static loading, piled rafts are a well-established foundation system (e.g. O'Neill et al., 1996; Poulos, 2001; Reul & Randolph, 2025). If applied to bridge foundations (e.g. Hecht & Dürrwang, 2001, Comodromos et al., 2016), lateral loads generally are of greater importance. However, in contrast to piled rafts under predominantly vertical loading, comparatively fewer investigations have been documented for piled rafts under combined vertical and lateral loading, regardless of whether monotonic, cyclic or dynamic actions are involved (Reul & Randolph, 2025).

In some recent studies, the behaviour of piled rafts under dynamic loading conditions was studied numerically using linear elastic-perfectly plastic soil models, which generate only elastic strains upon small-strain load reversals (e.g. Eslami et al., 2011; Kumar et al., 2016; Bhaduri & Choudhury, 2019; Akbari et al., 2021; El-Attar, 2021). However, the capability to realistically capture the main aspects of soil-structure interaction under dynamic loading requires the selection of more advanced constitutive models for the soil. For example, Zhang et al. (2017) and Mittal & Samanta (2025) used a hyperbolic-hysteretic soil model and Mohr-Coulomb failure criterion in conjunction with the modified hyperbolic model, respectively, to simulate nonlinear soil behaviour in their studies. The Hardening Soil model with small-strain stiffness (Benz, 2007), referred to as the HSsmall model in the remainder of this paper, captures small-strain stiffness and some inherent damping effects and is therefore suited for dynamic loading conditions.

The current research project aims on providing a better understanding of the bearing behaviour of piled rafts under lateral monotonic and dynamic loading by means of numerical simulations with the finite element method. In this paper, the bearing behaviour of piled rafts under combined vertical static and lateral seismic loading in dry Toyoura sand was investigated by means of three-dimensional finite element analysis (3D FEA) using the HSsmall model for the soil. The foundation and load configurations investigated in the parametric study are related to integral bridges.

2 NUMERICAL MODEL

2.1 *FE mesh and damping characteristics*

The numerical simulations were carried out with the program PLAXIS 3D (Plaxis bv, 2022). After conducting mesh sensitivity analyses, based on the convergence of the results and optimised computational time, a medium-sized mesh with additional refinement in the vicinity of the foundation was generated. As suggested by Kuhlemeyer & Lysmer (1973) for dynamic loading, the element sizes were smaller than 1/8 of the wavelength associated with the maximum frequency component of the input motion. A typical model comprising 155,000 10-node tetrahedral volume elements and 226,672 nodes, with an average element size of 1.35 m, fulfils this criterion. Figure 1a shows the FE mesh of the system, where 1/2 of the complete 3D problem was modelled considering one symmetry plane.

In previous studies, rafts and piles were frequently modelled as plate and embedded beam elements, respectively (e.g., Tschuchnigg, 2012; Kumar et al., 2016; Mali & Singh, 2018; Chanda et al., 2020; Jamil et al., 2023). However, to capture the complex interaction effects of the piled raft system more accurately, this study employs 10-node tetrahedral volume elements also for the piles and the raft. Instead of modelling the entire integral bridge, simplifications were made to the deck and the

pier. Consistent with other studies (e.g. Wang et al., 2017; Azizkandi et al., 2018; Alfach, 2023), a 5 m long cantilever beam was used to idealise the pier, and a 0.3 m thick plate was used to represent the bridge deck, with their masses lumped at the deck level (Figure 1b). The beam and the plate comprised 3-noded beam elements and 6-noded triangular plate elements, respectively. A rigid connection between the base of the pier and the raft was simulated by embedding the pier throughout the entire height of the raft.

The piles were installed "wished-in-place" in the FE model, which is considered to capture the installation process of cast-in-situ bored piles reasonably well (e.g. Reul & Randolph, 2025). Between the piled raft and the soil, 12-node interface elements with a designated interface strength reduction factor of $R_{inter} = 1$ to reflect rough concrete surfaces that were placed (Figure 1c). For the extraction of pile forces, zero-mass dummy beams with the same diameter as the piles but with stiffness reduced by a factor of 1000 were located in all piles (Figure 1c), leaving the axial and flexural stiffness of the piles unaltered.

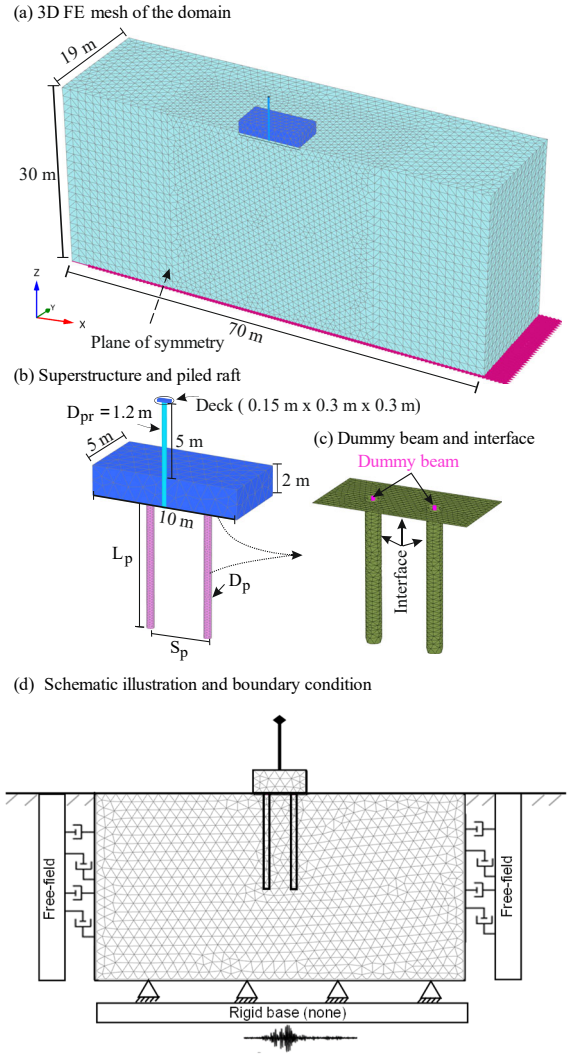

Figure 1. FE model.

Except for lateral boundaries in the direction of loading, all lateral and bottom model boundaries were constrained to restrict perpendicular movements. At the lateral boundaries in the direction of loading (Figure 1d), free-field boundary conditions were applied to account for energy dissipation (radiation/geometric damping) during dynamic loading. To account for material damping, Rayleigh damping with a target damping ratio $\xi = 2\%$ was considered, in addition to the geometric and hysteretic damping. Hysteretic damping is incorporated in the constitutive model of the soil (section 2.2). For comparison purposes, results using $\xi = 5\%$ are also included in some of the plots presented later, as this damping ratio is a typical value for the considered materials (Kramer, 1996). For the formulation of Rayleigh damping, the pier and the foundation system were idealised as a two-degree-of-freedom system (2-DOF). The mass proportional damping coefficient α and the stiffness proportional damping coefficient β of the Rayleigh damping were calculated from the first circular natural frequency of the 2-DOF system ω_1 and an odd multiple of it, $\omega_2 = n\omega_1$. Here n is the closest odd integer larger than the ratio ω_p/ω_1, where ω_p is the predominant circular frequency of the input motion (Hudson et al., 1994). Additionally, the natural frequencies were determined using an analytical approach according to Xu et al. (2016), which gave comparable results. The stiffness parameters used to determine the natural frequencies were established based on a simple cantilever beam model for the pier and on a formulation developed by Worku & Lulseged (2023) for the foundation system. Accordingly, the Rayleigh damping coefficients $\alpha = 0.443$ and $\beta = 6.78e^{-4}$ were determined and employed in the numerical analysis.

2.2 *Material properties*

The material behaviour of the dry Toyoura sand was modelled with the HSsmall model (Benz, 2007), which is an extension of the standard Hardening Soil (HS) model (Schanz et al., 1999), incorporating two additional parameters: the shear modulus at a very small strain G_0^{ref} and the threshold shear strain $\gamma_{0.7}$, the shear strain at which the secant shear modulus G_s^{ref} is degraded to $0.72 \cdot G_0^{ref}$. The material parameters of the HSsmall model for Toyoura sand summarised in Table 1 were calibrated by Degu et al. (2024) based on the back-analysis of the centrifuge model tests by Horikoshi et al. (2003a; 2003b). Since the pier, raft and piles are made of concrete, they are considered to behave linear elastically with the material parameters listed in Table 2.

Table 1. Material parameters of the soil (Degu et al., 2024).

Parameter			Toyoura sand
Dry unit weight	γ_d	kN/m³	15.2
Reference secant stiffness at 50% of q_f	E_{50}^{ref}	MPa	42.1
Tangent oedometric stiffness	E_{oed}^{ref}	MPa	30.2
Unloading-reloading stiffness	E_{ur}^{ref}	MPa	126.9
Unloading-reloading Poisson's ratio	ν_{ur}	-	0.2
Power for stress-level dependency of stiffness	m	-	0.65
Reference stress for stiffness	p^{ref}	kPa	100.0
Reference shear stiffness at very small strain	G_0^{ref}	MPa	149.0
Threshold shear strain at which $G_s = 0.722 \cdot G_0$	$\gamma_{0.7}$	-	1.2·10-4
Cohesion	c	kPa	5.8
Angle of internal friction	φ	°	35.6
Angle of dilatancy	ψ	°	8.7
Coefficient of earth pressure at rest for NC soil	K_0^{nc}	-	0.47
Failure ratio (q_f/q_a)	R_f	-	0.9
Initial void ratio	e_0	-	0.75

q_f & q_a= asymptotic and ultimate deviatoric stresses, respectively

Table 2. Material parameters of deck, pier, raft and piles.

Parameter			Deck	Pier	Pile	Raft
Unit weight	γ	kN/m³	*	0	25	25
Young's modulus	E	GPa	41.7	41.7	41.7	41.7
Poisson's ratio	ν	-	0.21	N/A	0.21	0.21

* Varies depending on the load case (Table 4)

2.3 *Foundation configurations in the parametric study*

In the parametric study, the piled raft comprises four piles and a square raft with an edge length of $b_r = 10$ m and a thickness of $t_r = 2$ m while the pile length L_p, the pile spacing S_p and the pile diameter D_p were varied as summarised in Table 3. The pile length selected for the analyses falls within the range of intermediate and long piles, as defined by Hetényi (1946) and Das (2016). The pile spacing was varied with $S_p \geq 2.5D_p$ in accordance with code requirements and other established guidelines (ASCE 20-96, 1997; Das, 2016). The pile diameters D_p used in the analyses fall within the range for bored piles, between $D_p = 0.3$ m and $D_p = 3.0$ m covered by DIN EN 1536 (2015).

Table 3. Pile dimensions.

Parameter			Variants			
Pile length	L_p	m	6	9	12	15
Pile spacing	S_p	m	2	4	6	8
Pile diameter	D_p	m	0.5	1.0	1.5	1.8

2.4 *Loading*

The vertical loads applied in the parametric study due to the weight of the deck and the raft are summarised in Table 4 and Table 6, respectively, with the load increase simulated by means of an increase in the unit weight of the deck. For comparison, the ultimate capacity of a single pile, assumed to be the resistance of the pile at a settlement equal to 10 % of the pile diameter as suggested by DN EN 1997-1 (2014), ranges between $R_{ult} = R(s = 0.1D_p) = 1094.2$ kN ($D_p = 0.5$ m ; $L_p = 9$ m) to $R_{ult} = 7{,}968.6$ kN ($D_p = 2.0$ m; $L_p = 12$ m).

Table 4. Vertical loads applied in the parametric study.

Load type			Load case			
			1	2	3	4
Load from the superstructure	P	kN	1,442	2,188	4,377	10,624
Increased unit weight of deck	γ_{deck}	kN/m³	53.4	81.1	162.1	393.5
Total load (Superstructure + raft)	$P_{\text{tot,v}}$	kN	6,442	7,188	9,377	15,624

The seismic load comprised an input motion of the 1989 Loma Prieta ground motion (CESMD, 2023; PEER, 2023), as presented in Figure 2 and Table 5. While the total duration of ground motion may not significantly affect the responses, the duration associated with strong ground motion is likely to have a greater impact. Bolt (1969), as cited in Kramer (1996), suggested the so-called bracketed duration as the time between the first and last exceedances of a threshold acceleration (usually 0.05g). In contrast, Trifunac & Brady (1975) defined the strong motion duration (referred to as the significant duration in this work) as the time interval between the points at which 5% and 95% of the total energy has been recorded.

The actual duration of the recorded accelerogram was $\Delta t = 40$ s; however, for optimum computational time, the duration was truncated to $\Delta t = 20$ s, as indicated in Figure 2, after confirming the negligible effects of truncation on the response of the pier-piled raft system. Moreover, the durations of the strong motion in an accelerogram, as defined e.g. by Bolt (1969) and Trifunac & Brady (1975) are within the truncated duration of $\Delta t = 20$ s. (Figure 2). Other researchers also used a truncated version of the same earthquake (e.g. Phanikanth et al., 2011; Floroiu, 2016).

Table 5. Main features of the input earthquake motion (1989 Loma Prieta earthquake; Gilroy Array #1, CA, USA)

Component	PGA	Duration	Time step	f_p
°	m/s²	s	s	Hz
90	4.3	20	0.02	2.7

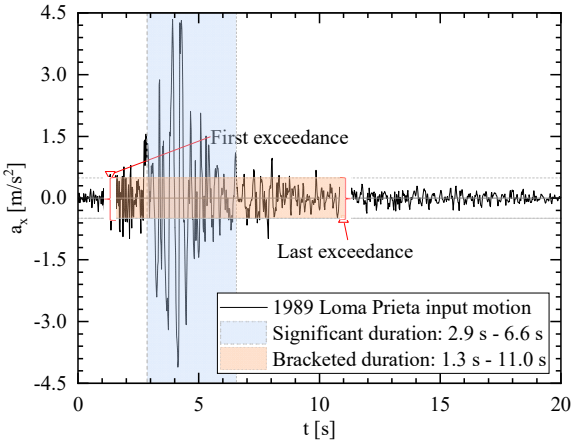

Figure 2. 1989 Loma Prieta input motion.

2.5 *Step-by-step analysis*

Table 6 summarises the step-by-step analysis in the numerical simulation. After the generation of the in-situ stress state by means of a K_0 procedure and the "wished-in-place" installation of piles and raft, the pier and the deck were included simultaneously in the model in step 4. The deck and other parts of the superstructure were represented by a lumped mass at the top of the pier, with the weight varying depending on the load case defined in Table 4. In the last step, a displacement-controlled seismic load excitation with a duration of $\Delta t = 20$ s was applied in form of a surface-prescribed displacement at the -rigid base.

In preliminary studies conducted by Degu (2026), appropriate tolerance and time step values were identified to ensure convergence of the results.

Table 6. Step-by-step analysis.

Step		$P_{tot,v}$ kN	Δt s	Calculation type as defined in Plaxis
1	In-situ stress state	-	-	K0 procedure
2	Pile installation	-	-	Plastic
3	Raft installation	5000	-	Plastic
4	Pier and deck installation	*1	-	Plastic
5	Vertical loading + lateral seismic load	*1	20	Dynamic*2

*1 Varies depending on the load case (Table 4)
*2 Displacements reset to zero prior to running step 5

3 RESULTS

The response of the piled raft and the superstructure, in terms of typical response spectra, peak acceleration, settlement and vertical piled raft coefficient, is presented in this section. The vertical piled raft coefficient α_{pr} is the ratio of the sum of the mobilised vertical pile resistances $\sum R_{pile,v}$, which is equal to the sum of the pile head axial forces $\sum N_{pile}$, to the total mobilised vertical resistance of the piled raft $R_{tot,v}$, which is equal to the total applied vertical load on the piled raft $P_{tot,v}$:

$$\alpha_{pr} = \frac{\sum R_{pile,v}}{R_{tot,v}} = \frac{\sum N_{pile}}{P_{tot,v}} \quad (1)$$

A piled raft coefficient of unity indicates a freestanding pile group, whereas a piled raft coefficient of zero describes a raft foundation.

The influence of the vertical load on the response of the piled raft is presented in Figure 3 and Figure 4. The settlement at the centre of the piled raft due to the seismic loading increases with increasing vertical load, with an abrupt increase observed during the significant duration of the input motion. Both before and after this significant duration, the settlement remains practically constant. The free-field motion, a motion without any interacting structure or far from it, also showed a settlement as a result of nonlinear soil behaviour caused by the seismic loading. Due to dynamic soil-structure interaction, an increase in irreversible settlement ranging from 54% to 91% of the free-field motion settlement was observed after the significant duration and continued through to the end of seismic loading (Figure 3), depending on the level of vertical load. Furthermore, the irreversible settlement caused by seismic loading increases by 262% to 906% relative to the irreversible settlement under static loading. Similar variations in settlement over time were reported in the literature (e.g., Horikoshi et al., 2003a; Takemura et al., 2014; Akbari et al., 2021).

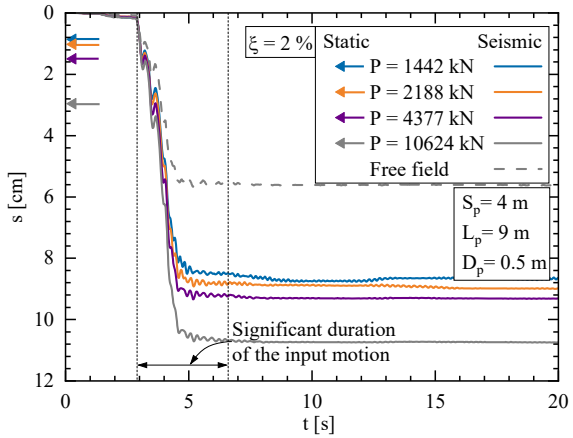

Figure 3. Influence of vertical load on raft centre settlement.

The variation of the horizontal pseudo-spectral acceleration PSA, expressed as a fraction of the acceleration due to gravity g, with the natural period T at the top of the pier (Figure 4), shows a significant decrease with increasing vertical load levels. This is attributed to the longer periods induced by the larger vertical loads. However, the predominant natural period T_p, i.e. the period corresponding to the peak value of the response, increases only slightly with the vertical load levels. Furthermore, the variation in spectral acceleration with natural period (i.e., the shape of the PSA plot), remains largely unaffected by changes in loading, except for the highest load level. The effect of the vertical load on the PSA at the raft top, which is not presented here for brevity, is not as pronounced as that at the pier top (Degu, 2026).

The effects of inertial and kinematic interactions are illustrated in Figure 5, which gives the horizontal pseudo-spectral acceleration at the raft-soil interface. When the weights of the piled raft and superstructure are neglected ($\gamma_{\text{deck+PR}} = 0.0$), inertial interaction is effectively eliminated. In this case, the PSA closely aligns with the free-field motion PSA, indicating negligible kinematic interaction effects. However, when the weight of the piled raft is considered ($\gamma_{\text{PR}} > 0$), while the superstructure weight remains neglected ($\gamma_{\text{deck}} = 0$), the spectral acceleration at the predominant period of the response increases by approximately 12% relative to the free-field PSA, emphasising the significance of inertial interaction.

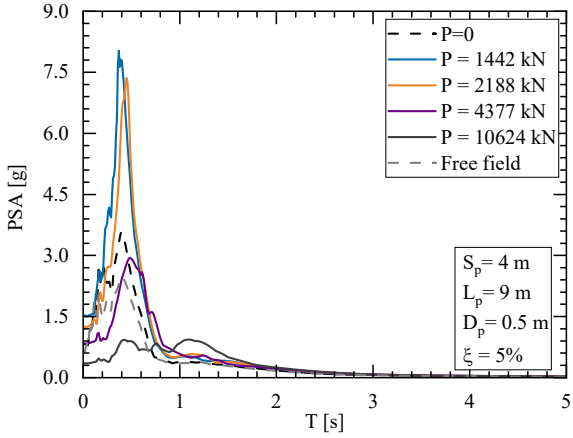

Figure 4. Influence of vertical load on the horizontal pseudo-spectral acceleration at the top of the pier.

Interestingly, when the weight of the superstructure is also included (Load case 3; $\gamma_{\text{deck+PR}} = 162.1\ \text{kN/m}^3 + 25.0\ \text{kN/m}^3$), the peak spectral acceleration decreases by approximately 8% compared to the free-field PSA. This reduction likely results from inertial interaction effects, specifically attributed to destructive interference between seismic waves propagating upward from the foundation and those reflected downward as a consequence of the inertial forces generated by the superstructure.

It is worth noting that the spectral curve of the input motion is lower than the remaining curves over almost the entire period range, showing the amplification regardless of the weight of the structure.

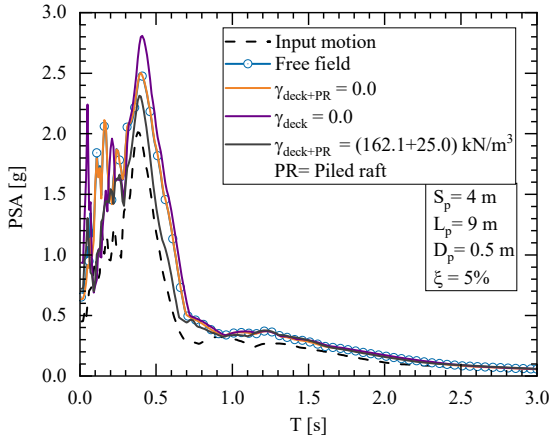

Figure 5. Inertial effects on the horizontal pseudo-spectral acceleration at the raft-soil interface.

The influence of pile spacing on the maximum acceleration at the top of the raft and pier is presented in Figure 6 for two target damping ratios. At both locations, the maximum acceleration slightly decreases with decreasing spacing, probably caused by the stress waves generated from the piles interacting with more destructive interference, decreasing the wave amplitude. Moreover, with closely spaced piles being located further away from the boundaries, the piles and the surrounding soil may experience higher radiation damping. Additionally, increased pile-pile interaction leads to stress overlap in between the piles and a shadowing effect, which can cause stiffness degradation around the piles due to the soil's nonlinear behaviour. This reduction in stiffness, in turn, may lead to an increase in the hysteretic damping for the closely spaced piles. Zhang et al. (2017)

and Varghese (2020) also reported a slight increase in raft acceleration with increasing pile spacing, as presented in the form of response spectral accelerations. Similar observations were reported by El-Attar (2021) for the peak acceleration.

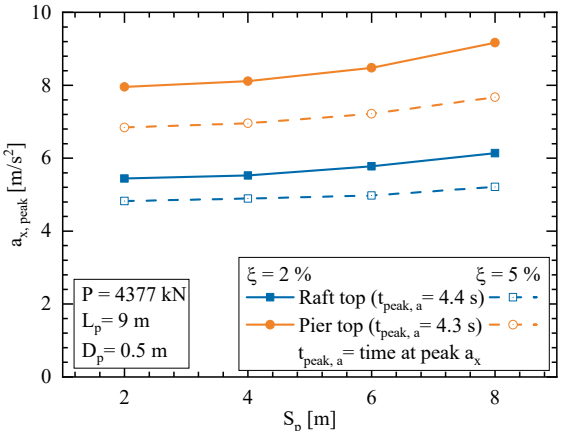

Figure 6. Influence of pile spacing on raft and pier top peak acceleration.

As depicted in Figure 7, the peak lateral displacement at the top of the pier relative to the raft top decreases with increasing spacing, consistent with the findings of Mittal & Samanta (2025). In contrast, El-Attar (2021) reported that the lateral displacement increases with spacing. It is worth noting that the time at which peak acceleration and peak lateral displacement at the top of the pier occur differs with $t_{peak,a} = 4.3$ s and $t_{peak,u} = 3.5$ s, respectively, resulting in different trends in the peak values of acceleration (Figure 6) and displacement (Figure 7) as spacing changes.

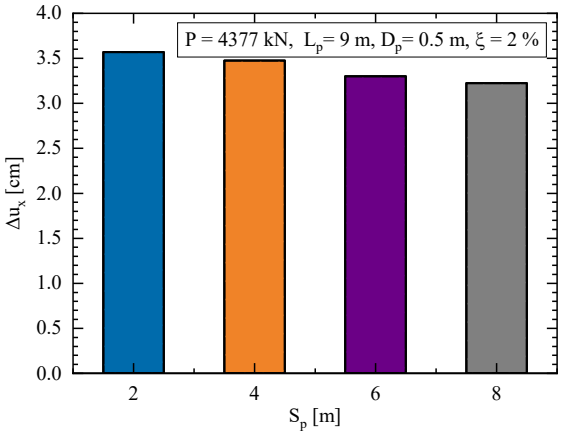

Figure 7. Influence of pile spacing on pier top peak lateral displacement.

Figure 8 shows the vertical piled raft coefficient increasing with increasing pile length. Moreover, the vertical piled raft coefficient before and after the significant duration varies depending on the length of the piles. For the pile length of $L_p = 12$ m and $L_p = 15$ m, the vertical piled raft coefficient increases during the significant duration and is almost constant before and after it, whereas for the shortest pile, a decrease is observed during the significant duration. This is probably attributed to an increase in confining pressure around the longer piles during shaking and a decrease in confining pressure around the shortest pile due to the mobilisation of its axial resistance. In contrast, shorter piles may reach full mobilisation of their capacity earlier, resulting in the transfer of the resistance to the raft. Variations in the load share before and after the earthquake were also reported by El-Attar (2021), with no clear trend for the effect of the pile length recognisable.

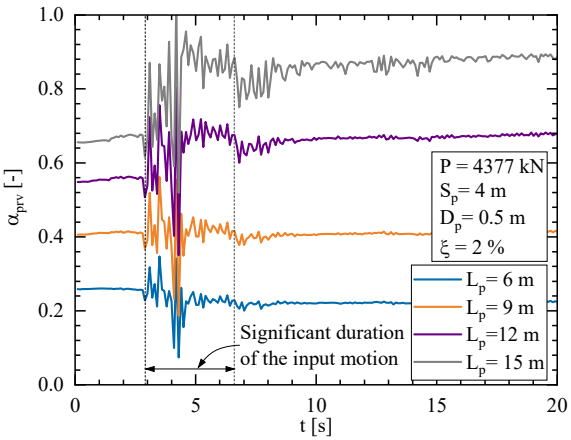

Figure 8. Influence of pile length on vertical piled raft coefficient.

The influence of the pile diameter is shown in Figure 9. As the diameter increases, other factors kept constant, the vertical piled raft coefficient during the significant duration also increases. For pile diameters of $D_p = 0.5$ m and $D_p = 1.0$ m, the vertical piled raft coefficient is nearly constant before and after the significant duration. This behaviour is likely due to an increase in the stiffness of the soil. This enhancement in soil properties, in turn, improves both shaft and base resistance of the pile, with the effect being more pronounced on the larger diameter piles ($D_p = 1.5$ m and $D_p = 1.8$ m). This may also contribute to pressure relief beneath the raft.

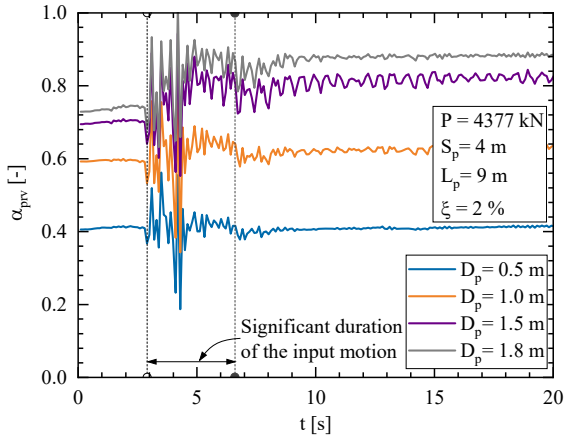

Figure 9. Influence of pile diameter on vertical piled raft coefficient.

The effect of pile spacing, not included here, on the vertical piled raft coefficient is minimal compared to the pile length and diameter discussed above (Degu, 2026). Additionally, an in-depth study has been conducted on a pile-supported bridge in Ethiopia as a case study (Degu, 2026). By considering the contribution of the raft in the load transfer, it was possible to reduce pile lengths significantly without compromising the requirements of SLS and ULS. As a result, significant cost savings were realised for the bridge.

4 CONCLUSIONS

In this study, the effects of the vertical load level and the pile configuration on the response of a bridge pier founded on a piled raft subjected to seismic loading were investigated by means of 3D FEA. It can be concluded that, regardless of the foundation configuration, the effects of the seismic action are most pronounced during the significant duration when most of the energy is transferred into the system. For the investigated configurations, an increase in the pile spacing yielded an increase in the peak acceleration of the raft, confirming the results

of previous studies. Moreover, dynamic soil-structure interaction effects were found to significantly influence the response of the structure-foundation system, with inertial interaction exhibiting a particularly strong impact. The next steps in the research project include the application of these findings to bridges founded on piled rafts to optimise the foundation configuration.

5 ACKNOWLEDGEMENTS

This work was financially supported by Bahir Dar University, the Catholic Academic Exchange Service, the Ethiopian Ministry of Education, the German Academic Exchange Service, and the University of Kassel. The authors are grateful for the financial support.

6 REFERENCES

Akbari, A., Eslami, A. and Nikookar, M., 2021. Influence of soil stiffness on the response of piled raft foundations under earthquake loading. *Transp. Infrastructure Geotechnology*, 8(4), 590–606.

Alfach, M. T., 2023. 3D numerical analysis of seismic interaction between 3 adjacent bridges via nonlinear soil. *Geotechnical and Geological Engineering*, 41(6), 3459–3494.

ASCE 20-96, 1997. *Standard guidelines for the design and installation of pile foundations*. ASCE, Virginia, USA.

Azizkandi, A. S., Baziar, M. H. and Yeznabad, A. F., 2018. 3D dynamic finite element analyses and 1g shaking table tests on seismic performance of connected and nonconnected piled raft foundations. *KSCE J. of Civil Engineering*, 22(5), 1750–1762.

Benz, T., 2007. *Small-strain stiffness of soils and its numerical consequences*. PhD thesis. Universität Stuttgart.

Bhaduri, A. and Choudhury, D., 2019. Influence of connection rigidity on combined pile-raft foundation under seismic loading. *Proc. 7th Int. Conf. on Earthquake Geot. Engineering*. Rome, Italy, 1437–1444.

Bolt, B. A., 1969. Duration of strong motion. *Proc. 4th World Conf. on Earthquake Engineering*. Santiago, Chile, 1304–1315.

CESMD, 2023. *Center for Engineering Strong Motion Data: Strong-Motion Virtual Data Center(VDC)*. Online: https://www.strongmotioncenter.org.

Chanda, D., Saha, R. and Haldar, S., 2020. Behaviour of piled raft foundation in sand subjected to combined V-M-H loading. *Ocean Engineering*, 216.

Comodromos, E. M., Papadopoulou, M. C. and Laloui, L., 2016. Contribution to the design methodologies of piled raft foundations under combined loadings. *Can. Geot. J.*, 53(4), 559–577.

Das, B. M., 2016. *Principles of foundation engineering*. 8th ed. Boston, USA: Cengage learning.

Degu, Y., Reul, O., Worku, A. and Tschuchnigg, F., 2024. Calibration of a numerical model for the investigation of piled rafts under dynamic loading. *Proc. XVIII Europ. Conf. on Soil Mechanics and Geotechnical Engineering*. Lisbon, Portugal. London: CRC Press, 1560–1565.

Degu, Y., 2026. *Bearing behaviour of piled rafts under lateral static and dynamic loading*. PhD thesis. Universität Kassel. (Under preparation).

DIN EN 1536, 2015. *Ausführung von Arbeiten im Spezialtiefbau - Bohrpfähle*. Normenausschuss Bauwesen (NABau) im DIN

DN EN 1997-1, 2014. *Eurocode 7: Entwurf, Berechnung und Bemessung in der Geotechnik - Teil 1: Allgemeine Regeln*. Normenausschuss Bauwesen (NABau) im DIN

El-Attar, A., 2021. Dynamic analysis of combined piled raft system. *Ain Shams Engineering J.*, 12(3), 2533–2547.

Eslami, M. M., Aminikhah, A. and Ahmadi, M. M., 2011. A comparative study on pile group and piled raft foundations (PRF) behavior under seismic loading. *Computational Methods in Civil Engineering*, 2(2), 185–199.

Floroiu, L.-G., 2016. *A contribution to seismic ground response of improved foundation soil*. PhD thesis. Graz University of Technology.

Hecht, T. and Dürrwang, R., 2001. Optimierung der Gründung der Reichenbachtalbrücke mit der Kombinierten Pfahl-Plattengründung *Proc. of Pfahl-Symposium*. Braunschweig, Germany, 21–34.

Hetényi, M., 1946. *Beams on elastic foundation: theory with applications in the fields of civil and mechanical engineering*. Michigan, USA: University of Michigan Press.

Horikoshi, K., Matsumoto, T., Hashizume, Y. and Watanabe, T., 2003a. Performance of piled raft foundations subjected to dynamic loading. *Int. J. of Physical Modelling in Geotechnics*, 3(2), 51–62.

Horikoshi, K., Matsumoto, T., Hashizume, Y., Watanabe, T. and Fukuyama, H., 2003b. Performance of piled raft foundations subjected to static horizontal loads. *Int. J. of Physical Modelling in Geotechnics*, 3(2), 37–50.

Hudson, M., Idriss, I. M. and Beikae, M., 1994. *User's Manual for QUAD4M.* California, USA.

Jamil, I., Ahmad, I., Khan, I., Ullah, W., Ur Rehman, A. and Ali Khan, S., 2023. Factors affecting the lateral contribution of a raft in a piled raft system. *Ain Shams Engineering J.*, 14(5).

Kramer, S. L., 1996. *Geotechnical earthquake engineering*. New Jersey, USA: Prentice-Hall.

Kuhlemeyer, R. L. and Lysmer, J., 1973. Finite element method accuracy for wave propagation problems. *J. of the Soil Mechanics and Foundations Division*, 99(5), 421–427.

Kumar, A., Choudhury, D. and Katzenbach, R., 2016. Effect of earthquake on combined pile-raft foundation. *Int. J.of Geomechanics*, 16(5). 04016013:1–16

Mali, S. and Singh, B., 2018. Behavior of large piled-raft foundation on clay soil. *Ocean Engineering*, 149, 205–216.

Mittal, V. and Samanta, M., 2025. Influence of Spacing and Slenderness Ratio of End-Socketed Pile Foundation on Seismic Response of Building Considering Soil-Pile-Structure Interaction: An Experimental Approach. *J. of Structural Engineering*, 151(2).

O'Neill, M. W., Caputo, V., De Cock, F., Hartikainen, J. and Mets, M., 1996. *Case histories of pile-supported rafts*. Report for ISSMFE TC18, University of Houston, Texas.

PEER, 2023. *PEER Strong Ground Motion Databases*. Online: https://peer.berkeley.edu/peer-strong-ground-motion-databases.

Phanikanth, V. S., Choudhury, D. and Rami Reddy, G., 2011. Equivalent-linear seismic ground response analysis of some typical sites in Mumbai. *Geotechnical and Geological Engineering*, 29, 1109–1126.

Plaxis bv, 2022. *Plaxis 3D - Software*. 22nd ed. Delft, the Netherlands: Plaxis bv, Bentley Systems, Incorporated.

Poulos, H. G., 2001. Piled raft foundations: design and applications. *Géotechnique*, 51(2), 95–113.

Reul, O. and Randolph, M., 2025. *Combined pile-raft foundations: Design and practice*. London: CRC Press.

Schanz, T., Vermeer, P. A. and Bonnier, P. G., 1999. The hardening soil model: formulation and verification. *1st int. Plaxis symposium*. the Netherlands: CRC Press, 281–296.

Takemura, J., Yamada, M. and Seki, S., 2014. Dynamic response and settlement behavior of piled raft foundation of oil storage tank. *Proc. 8th Int. Conf. on Physical Modelling in Geotechnics 2014*. Perth, Australia, CRC Press, 613–619.

Trifunac, M. D. and Brady, A. G., 1975. A study on the duration of strong earthquake ground motion. *Bulletin of the Seismological Society of America*, 65(3), 581–626.

Tschuchnigg, F., 2012. *3D finite element modelling of deep foundations employing an embedded pile formulation*. PhD Thesis. Graz University of Technology.

Varghese, R., 2020. *Kinematic and inertial response of piled raft foundations numerical and experimental studies*. PhD thesis. Indian Institute of Technology.

Wang, R., Liu, X. and Zhang, J.-M., 2017. Numerical analysis of the seismic inertial and kinematic effects on pile bending moment in liquefiable soils. *Acta Geotechnica*, 12(4), 773–791.

Worku, A. and Lulseged, A., 2023. Lateral static response of piles based on a full-fledged two-parameter foundation model. *Int. J. of Geomechanics*, 23(2).

Xu, Y., Shang, Y. and Ye, A., 2016. Dynamic interaction between bridge pier and its large pile foundation considering earthquake and scour depths. *Advances in structural engineering*, 19(9), 1390–1402.

Zhang, L., Goh, S. H. and Liu, H., 2017. Seismic response of pile-raft-clay system subjected to a long-duration earthquake: centrifuge test and finite element analysis. *Soil Dynamics and Earthquake Engineering*, 92, 488–502.